Vascular smooth muscle cell culture in microfluidic devices

Y. C. Wei,[1,a)] F. Chen,[2,a)] T. Zhang,[2,3,a)] D. Y. Chen,[1] X. Jia,[2] J. B. Wang,[1,b)] W. Guo,[2,b)] and J. Chen[1,b)]
[1]*State Key Laboratory of Transducer Technology, Institute of Electronics, Chinese Academy of Sciences, Beijing, People's Republic of China*
[2]*Department of Vascular Surgery, Clinical Division of Surgery, Chinese PLA General Hospital, Beijing, People's Republic of China*
[3]*Department of Vascular Surgery, Peking University People's Hospital, Beijing, People's Republic of China*

(Received 19 May 2014; accepted 13 August 2014; published online 25 August 2014)

This paper presents a microfluidic device enabling culture of vascular smooth muscle cells (VSMCs) where extracellular matrix coating, VSMC seeding, culture, and immunostaining are demonstrated in a tubing-free manner. By optimizing droplet volume differences between inlets and outlets of micro channels, VSMCs were evenly seeded into microfluidic devices. Furthermore, the effects of extracellular matrix (e.g., collagen, poly-L-Lysine (PLL), and fibronectin) on VSMC proliferation and phenotype expression were explored. As a platform technology, this microfluidic device may function as a new VSMC culture model enabling VSMC studies. [http://dx.doi.org/10.1063/1.4893914]

I. INTRODUCTION

Vascular smooth muscle cells (VSMCs) are essential blood vessel components responsible for the regulation of vessel tones and their dysfunctions may lead to diverse vascular diseases[1,2] (e.g., abdominal aortic aneurysm,[3,4] atherosclerosis,[5–7] and restenosis[8,9]). Current studies of VSMCs are based on conventional cell culture approaches (e.g., culture dish and flask),[10,11] which allow no control over the spatial/temporal distribution of the cells and biomolecules and thus cannot recapitulate local *in vivo* microenvironments.

Microfluidics is the science and technology of manipulating and detecting fluids in the microscale.[12,13] Due to its dimensional comparison with biological cells and capabilities of defining local biophysical, biochemical, and physiological cues, microfluidics has been used to construct more *in vivo* like cell culture models,[14–16] enabling tumor,[17,18] neuron,[19] and vascular[20,21] studies.

As to applications of microfluidics to vascular smooth muscle cell studies, preliminary studies were confined within three areas.[22–43] As the first demonstration, soft lithography was used to form micro and nano patterned extracellular matrix proteins and geometrical topographies enabling the regulation of VSMC morphologies and phenotypes.[22,23,27–31,36,37,39] Furthermore, microfluidics based gradient-compliance substrates were proposed to investigate durotaxis (migration from less stiff to more stiff substrates) of VSMCs.[26,35] Meanwhile, three-dimensional culture of VSMCs based on layer-by-layer assemblies[32,38] or circular micro channels[42] were demonstrated for tissue engineering studies. However, the combination of microfluidics with vascular smooth muscle cells is still at an early stage and no systematic studies of on-chip VSMC culture were previously demonstrated.

[a)]Y. C. Wei, F. Chen, and T. Zhang contributed equally to this work.
[b)]Authors to whom correspondence should be addressed. Electronic addresses: jbwang@mail.ie.ac.cn, Tel./Fax: 86-10-58887191; pla301dml@vip.sina.com, Tel./Fax: 86-10-66938349; and chenjian@mail.ie.ac.cn, Tel./Fax: 86-10-58887531/32-816.

To address this issue, this paper proposed a microfluidic platform for VSMC culture where extracellular matrix coating (Figures 1(a) and 1(b)), VSMC seeding, culture and observation (Figures 1(c)–1(e)), and immunostaining (Figures 1(f)–1(h)) are demonstrated in a tubing-free manner. More specifically, the VSMC seeding evenness in microfluidic channels was investigated and the effects of extracellular matrix on VSMC phenotypes were explored. In addition, as gravity was used as the driving force for cell loading and immunostaining, this platform does not need external pumps and tubes, which can be operated in biological labs with low access requirements.

II. MATERIALS AND METHODS

A. Materials

Dulbecco Modified Eagle Medium (DMEM) was purchased from Hyclon and the other cell-culture reagents were purchased from Life Technologies. SU-8 photoresist (MicroChem) was used for mold master fabrication while collagen (Sigma), poly-L-Lysine (PLL) (Sigma), and fibronectin (Sigma) were used for glass surface coating. Materials for alpha actin immunostaining included 4% paraformaldehyde (Sigma), primary antibody (Bioss), GTVision Detection System (Gene Technology), and goat serum (GIBCO).

B. Device design and fabrication

Polydimethylsiloxane (PDMS) based microchannels with channel dimensions of $10.00\,\mathrm{L} \times 0.80\,\mathrm{W} \times 0.10\,\mathrm{H}$ (mm) were proposed in this study, where each channel was divided into eight observation windows ($1.00\,\mathrm{L} \times 0.80\,\mathrm{W} \times 0.10\,\mathrm{H}$ (mm)) and labeled as 1 to 8 for cell distribution eveness evaluation. Two microchannel ports (channel inlet and outlet) with a diameter of 4 mm and a PDMS thickness of 2 mm were used in this study to facilitate liquid droplet manipulation. Four channels were included in one mask to characterize operation repeatability (see Figure 2(a)).

The PDMS device was replicated from a single-layer SU-8 mold based on the conventional soft lithography (see Figure 2(b)). Briefly, SU-8 5 was spin coated on a glass slide, flood exposed, post exposure baked, and hard baked (without development) to form an adhesive layer, followed by SU-8 2100 spin coating, exposure and development, forming the mold master with a height of 100 μm. PDMS prepolymers and curing agents were mixed, degassed, poured on channel masters, and baked in an oven. Cured PDMS channels were then peeled from the SU-8 masters with ports punched through and bonded to glass slides.

C. Cell culture

VSMCs of CRL-1999 (ATCC) were cultured with DMEM media supplemented with 10% fetal bovine serum and 1% penicillin and streptomycin. Immediately prior to an experiment, cells were trypsinized, centrifuged, and resuspended in supplemented culture medium with a concentration of 1×10^6 cells per ml. Cell passage generations between p6 and P12 were used in the experiments.

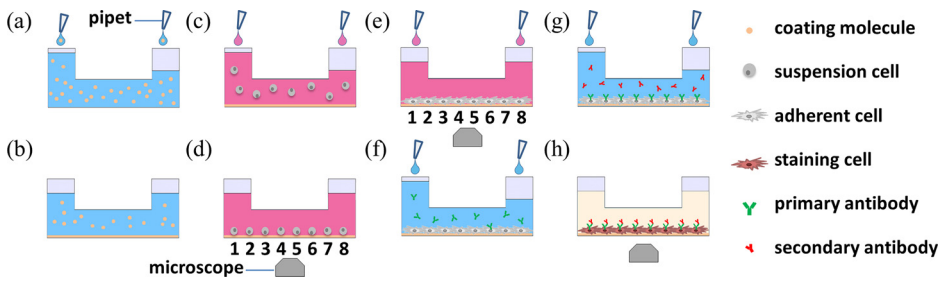

FIG. 1. Schematic of the tubing-free microfluidic platform for vascular smooth muscle cell (VSMC) culture where gravity was used for extracellular matrix coating ((a) and (b)), VSMC seeding, culture and observation ((c)-(e)), and immunostaining ((f)-(h)).

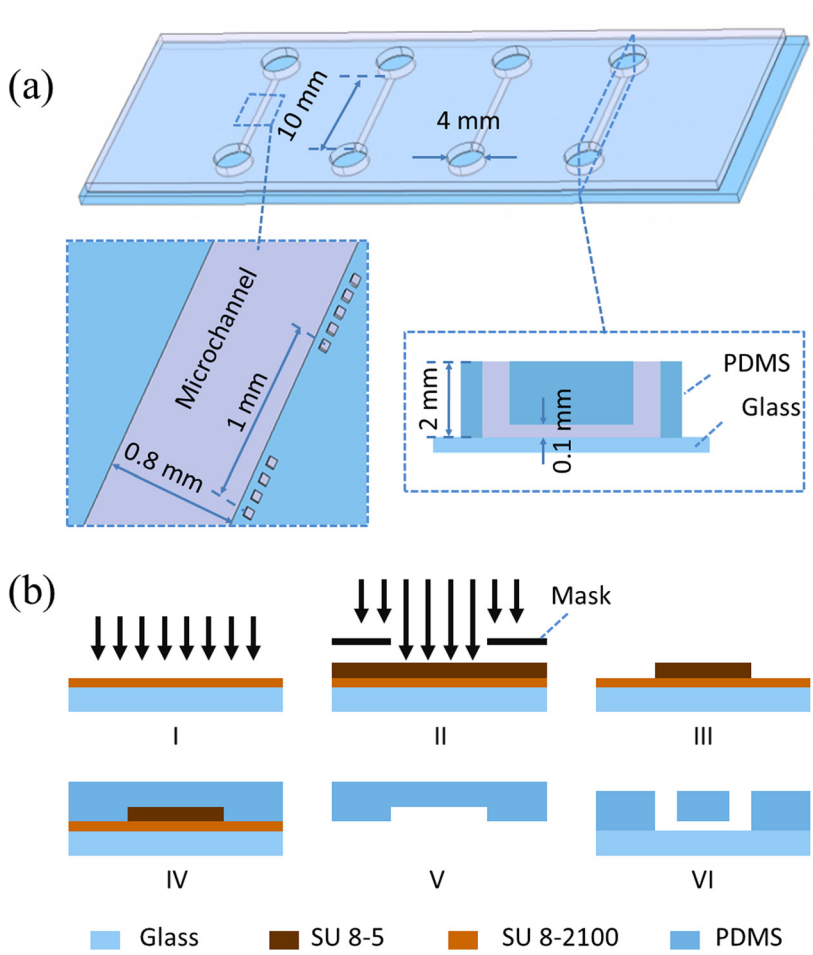

FIG. 2. (a) Dimensions of microfluidic devices for VSMC culture (channel length: 10 mm, channel width: 0.8 mm, channel height: 0.1 mm, port diameter: 4 mm, PDMS thickness: 2 mm). (b) Microfluidic device fabrication flow chart including SU-8 5 based adhesive layer fabrication (I), channel mold master fabrication using SU-8 2100 (II, III), PDMS channel structure formation (IV, V), and PDMS-glass bonding (VI).

D. Device operation and data analysis

The fabricated microfluidic devices were sterilized in a hood under ultraviolet (UV) overnight, followed by surface coating (PLL of 0.1 mg per ml, or fibronectin of 0.1 mg per ml or collagen of 1 mg per ml). As the first step, phosphate-buffered saline (PBS) solutions were flushed into the microfluidic devices by using micro pipets. Then, PBS solutions in two ports were replaced with coating solutions containing PLL, fibronectin, or collagen at a volume of 20 μl and 15 μl, respectively. Due to the gravity difference, the coating solutions were loaded into microfluidic channels for one-hour channel soaking. In the end, the coating solutions were removed by aspiration and the coated surfaces were rinsed with DMEM thoroughly.

The cell loading and observation protocol is as follows. DMEM solutions in two ports were removed and replaced with cell suspension solutions at 20 vs. 18 μl, 20 vs. 15 μl, 20 vs. 10 μl or 20 vs. 0 μl, respectively (1×10^6 cells per ml). After five minutes of cell loading, microscopic images were taken to evaluate the cellular seeding evenness. Then each microfluidic device was placed in a petri dish containing PBS to limit evaporation and osmolality shifts and then incubated in a cell incubator. DMEM was replaced every 12 h where solutions in two ports were removed and replaced with 20 μl fresh culture medium.

The on-chip immunostaining procedure is as follows. Cells within microfluidic devices were washed twice with PBS, fixed by 4% paraformaldehyde (15 min), permeabilized by 0.3%

Triton X-100 (15 min), blocked with 10% goat serum (1 h). Then cells within microfluidic devices were incubated with primary antibodies (1:100) at 37 °C (1 h), secondary antibodies at 37 °C (1 h), and the Diaminobenzidine (DAB) solution (2 min), sequentially. Note that in all the steps requiring liquid handling, a setup of 20 vs. 10 μl was used where gravity was the driving force for liquid manipulation inside microfluidic devices.

In order to evaluate the cell loading evenness and the cellular proliferation status inside microfluidic channels, cell number analysis was conducted based on manual processing of phase-contrast images taken along the length of the micro channels at 0 h, 12 h, 24 h, 48 h, and 72 h ($\times$10 magnification and 592 images in total).

III. RESULTS AND DISCUSSION

Microfluidic technologies hold great promise for the creation of advanced cell culture models.[14–16] However, the majority of currently available microfluidic cell culture approaches are not compatible with existing laboratories since syringe pumps and plastic tubes are used for cell loading and liquid dispersion. In addition, these physical connections with microfluidic devices lead to cell seeding on tubing walls and medium instabilities due to tubing disturbances.[44,45]

To address this issue, Beebe *et al.*[44–46] and Takayama *et al.*[47–49] proposed the concept of tubing-free microfluidic cell culture where surface tension or gravity was used for cell loading and liquid manipulation. Based on surface tension, difference in menisci of unequal volumes of two drops is used to drive liquid flow, which was extensively optimized and demonstrated for cellular micro environment reconstructions.[44–46] Meanwhile, although gravity based cell loading (relying on the height rather than menisci difference of drops for the channel inlet and outlet) was utilized for cell loading and characterization,[47–49] corresponding operation optimization and condition investigation were not reported.

A. Cell loading distribution evaluation in microfluidic channels

Figure 3 shows the effects of liquid volume differences (different gravity levels) between two ports on the cell distribution evenness within microfluidic channels. For the microfluidic channels with a total volume of $\sim$1 μl and a cell loading concentration of 1 million cells per ml, solutions within two ports were replaced with 20 vs. 18 μl, 20 vs. 15 μl, 20 vs. 10 μl, or 20 vs. 0 μl, respectively.

Cell loading densities based on the setup of 20 vs. 18 μl were quantified as $94.2 \pm 21.7/\text{mm}^2$ (position 1), $103.3 \pm 23.6/\text{mm}^2$ (position 2), $85.4 \pm 12.6/\text{mm}^2$ (position 3), $79.6 \pm 20.7/\text{mm}^2$ (position 4), $81.7 \pm 17.8/\text{mm}^2$ (position 5), $67.9 \pm 10.4/\text{mm}^2$ (position 6), $65.8 \pm 6.8/\text{mm}^2$ (position 7), $56.7 \pm 4.8/\text{mm}^2$ (position 8), and $79.3 \pm 21.7/\text{mm}^2$ in average.

A trend in cell density decrease from the port loaded with 20 μl to the port loaded with 18 μl was observed as $94.2 \pm 21.7/\text{mm}^2$ (position 1) vs. $56.7 \pm 4.8/\text{mm}^2$ (position 8) (Figures 3(a) and 3(e)). These experiments show that the 2 μl volume difference between two ports was not capable of pushing the cell solution through the whole microfluidic channel, which was confirmed by the observation of a significant decrease in concentrations of the suspended cells in the downstream of the microfluidic channel (positions 7 and 8).

Cell loading densities for the setup of 20 μl vs. 15 μl were quantified as $105.0 \pm 18.1/\text{mm}^2$ (position 1), $100.2 \pm 20.8/\text{mm}^2$ (position 2), $94.6 \pm 13.7/\text{mm}^2$ (position 3), $100.9 \pm 17.0/\text{mm}^2$ (position 4), $91.6 \pm 16.3/\text{mm}^2$ (position 5), $94.6 \pm 15.9/\text{mm}^2$ (position 6), $91.8 \pm 9.7/\text{mm}^2$ (position 7), $89.6 \pm 8.2/\text{mm}^2$ (position 8), and $96.0 \pm 16.3/\text{mm}^2$ in average.

This is the optimal choice since the averaged cell density ($96.0 \pm 16.3/\text{mm}^2$) approaches the idea cell loading density of $100/\text{mm}^2$ and the ratio of standard deviation to average was the lowest among all the four setups (Figures 3(b) and 3(e)). In this setup, cell suspension solutions were assumed to replace the culture medium solutions inside microfluidic channels thoroughly as the first step, followed by cell seeding on the substrates.

Cell loading densities for the setup of 20 μl vs. 10 μl were quantified as $220.8 \pm 36.7/\text{mm}^2$ (position 1), $209.2 \pm 13.8/\text{mm}^2$ (position 2), $184.2 \pm 15.9/\text{mm}^2$ (position 3), $162.5 \pm 10.2/\text{mm}^2$

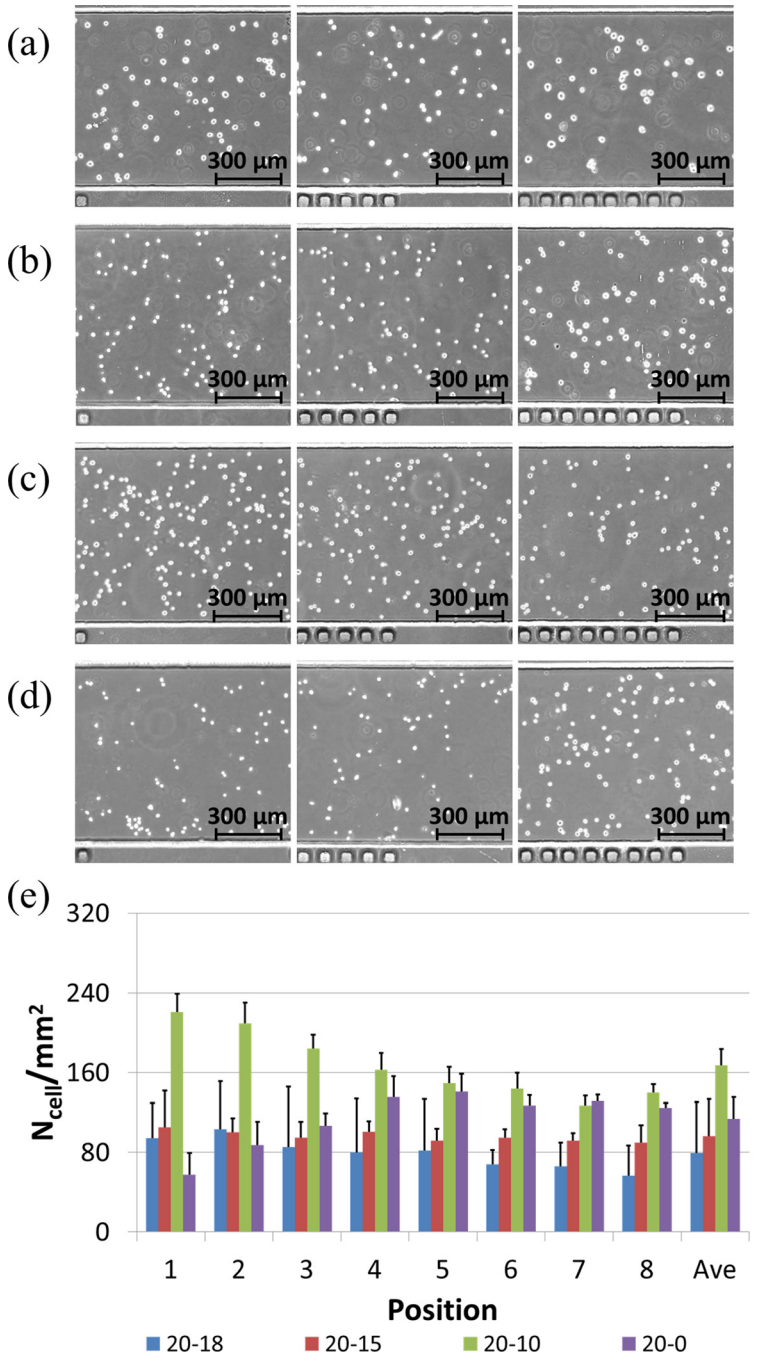

FIG. 3. Microscopic pictures of seeded VSMCs at positions of 1, 5, and 8 (left to right) for 20 vs. 18 μl (a), 20 vs. 15 μl (b), 20 vs. 10 μl (c), and 20 vs. 0 μl (d), respectively, with quantified cell numbers (e). These results suggest an optimal choice of the 20 vs. 15 μl setup for even cell distribution.

(position 4), $149.2 \pm 12.3/mm^2$ (position 5), $143.7 \pm 8.4/mm^2$ (position 6), $127.1 \pm 7.4/mm^2$ (position 7), $140.0 \pm 17.4/mm^2$ (position 8), and $167.1 \pm 37.2/mm^2$ in average.

A trend in cell density decrease from the port loaded with 20 μl to the port loaded with 10 μl was observed ($220.8 \pm 36.7/mm^2$ (position 1) vs. $140.0 \pm 17.4/mm^2$ (position 8)) (Figures 3(c) and 3(e)). In addition, the quantified averaged cell density number was much higher than the ideal cell loading density ($167.1 \pm 37.2/mm^2$ vs. $100/mm^2$). The 10 μl volume difference may lead to a prolonged cell flushing process. As the cell suspension solution was

flushed from position 1 to position 8, there was a concentration decrease due to the concurrent cell seeding process, which results in lower cell seeding densities in the downstream of microfluidic channels compared to upstream counterparts.

Cell loading densities for the setup of 20 μl vs. 0 μl were quantified as $57.5 \pm 35.5/\text{mm}^2$ (position 1), $87.2 \pm 47.9/\text{mm}^2$ (position 2), $106.6 \pm 60.7/\text{mm}^2$ (position 3), $135.3 \pm 54.2/\text{mm}^2$ (position 4), $140.9 \pm 51.5/\text{mm}^2$ (position 5), $126.9 \pm 14.4/\text{mm}^2$ (position 6), $131.3 \pm 23.8/\text{mm}^2$ (position 7), $124.7 \pm 30.1/\text{mm}^2$ (position 8), and $113.8 \pm 51.1/\text{mm}^2$ in average.

A trend in cell density increase from the port loaded with 20 μl to the port loaded with 0 μl was located ($57.5 \pm 35.5/\text{mm}^2$ (position 1) vs. $124.7 \pm 30.1/\text{mm}^2$ (position 8)) (Figures 3(d) and 3(e)). It was speculated that the 20 μl volume difference lead to a prolonged cell flushing process, together with cellular seeding on micro channels. Due to the existence of the 20 μl volume difference, a higher flow rate compared to the setup of 20 μl vs. 10 μl was produced, which lead to cell settlement in the downstream rather than in the upstream of microfluidic channels. Thus a higher cell seeding density in position 8 than position 1 was recorded.

B. Effect of extracellular matrix on VSMC phenotypes

VSMCs have been demonstrated to have contractile or synthetic phenotypes.[11,50] Contractile VSMCs are featured with limited proliferation capabilities while synthetic VSMCs are characterized by high proliferation and extracellular matrix secretion. In the local microenvironments of VSMCs, extracellular matrix of fibronectin and collagen were located and their effects on VSMC phenotypes were investigated in conventional cell culture models.[51,52] This study was designed to investigate the effects of extracellular matrix on the phenotypes of VSMCs in the microfluidic environment.

Figure 4(a) shows the microscopic images of VSMCs cultured on the glass substrate without modifications in a time sequence, followed by an endpoint immunostaining of alpha actin filaments. Based on the manual cell counting, the cell numbers were quantified as $88.5 \pm 17.9/\text{mm}^2$ (12 h), $87.7 \pm 21.6/\text{mm}^2$ (24 h), $94.5 \pm 24.5/\text{mm}^2$ (48 h), and $102.4 \pm 28.5/\text{mm}^2$ (72 h) (see Figure 4(b)).

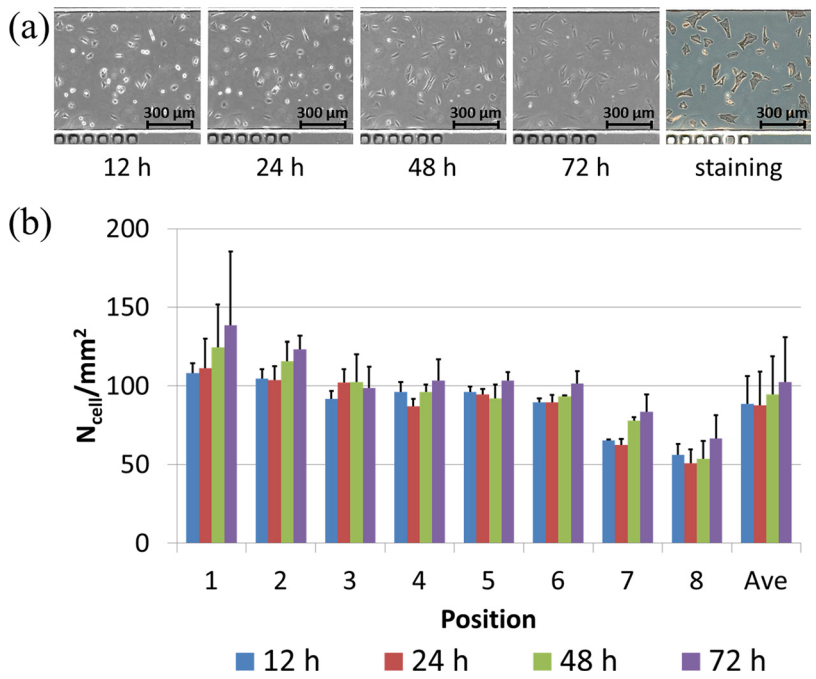

FIG. 4. (a) Microscopic pictures of VSMCs cultured on bare glass surfaces without modification in a time sequence (12 h, 24 h, 48 h, and 72 h (left to right)), followed by endpoint immunostaining of alpha actin filaments. (b) Cell numbers were quantified as $88.5 \pm 17.9/\text{mm}^2$ (12 h), $87.7 \pm 21.6/\text{mm}^2$ (24 h), $94.5 \pm 24.5/\text{mm}^2$ (48 h), and $102.4 \pm 28.5/\text{mm}^2$ (72 h).

Within the first 24 h of cell seeding, VSMCs were noticed to have limited surface spreading areas and no cellular proliferations ($88.5 \pm 17.9/mm^2$ (12 h) vs. $87.7 \pm 21.6/mm^2$ (24 h)) due to the bare glass surface without extracellular matrix coating. Starting from 24 h after cell seeding, VSMCs were noticed to increase in surface spreading areas with noticeable cellular proliferations from $87.7 \pm 21.6/mm^2$ (24 h) to $102.4 \pm 28.5/mm^2$ (72 h).

It was speculated that within the first 24 h, VSMCs secreted extracellular matrix macromolecules on glass substrates as extracellular modifications, which lead to cellular proliferations from 24 h to 72 h. These results indicate that VSMCs maintained the synthetic phenotype during the on-chip culture process, featured with extracellular molecule secretions and cellular proliferations.

Figure 5(a) shows the microscopic images of VSMCs cultured on collagen coated glass substrates in a time sequence, followed by an endpoint immunostaining of alpha actin filaments. Based on the manual cell counting, the cell numbers were quantified as $93.4 \pm 13.2/mm^2$ (12 h), $106.7 \pm 12.9/mm^2$ (24 h), $112.7 \pm 13.9/mm^2$ (48 h), and $111.3 \pm 13.4/mm^2$ (72 h) (see Figure 5(b)).

Within the first 48 h of cell seeding, noticeable VSMC proliferations were located with quantified cell numbers increased from $93.4 \pm 13.2/mm^2$ (12 h) to $106.7 \pm 12.9/mm^2$ (48 h), as an indicator of the synthetic phenotype. From 48 h to 72 h, no significant cellular proliferation was noticed ($112.7 \pm 13.9/mm^2$ (48 h) vs. $111.3 \pm 13.4/mm^2$ (72 h)), suggesting that VSMCs change from the synthetic phenotype to the contractile phenotype.

Figure 6(a) shows the microscopic images of VSMCs cultured on PLL coated glass substrates in a time sequence, followed by an endpoint immunostaining of alpha actin filaments. Based on the manual cell counting, the cell numbers were quantified as $150.1 \pm 33.2/mm^2$ (12 h), $166.2 \pm 42.1/mm^2$ (24 h), $188.1 \pm 70.2/mm^2$ (48 h), and $173.6 \pm 62.9/mm^2$ (72 h) (Figure 6(b)).

Within the first 48 h of cell seeding, noticeable VSMC proliferations were located with quantified cell numbers increased from $150.1 \pm 33.2/mm^2$ (12 h) to $188.1 \pm 70.2/mm^2$ (48 h), as an indicator of the synthetic phenotype. From 48 h to 72 h, a decrease in cellular proliferation was noticed ($188.1 \pm 70.2/mm^2$ (48 h) vs. $173.6 \pm 62.9/mm^2$ (72 h)), suggesting that VSMCs change from the synthetic phenotype to the contractile phenotype.

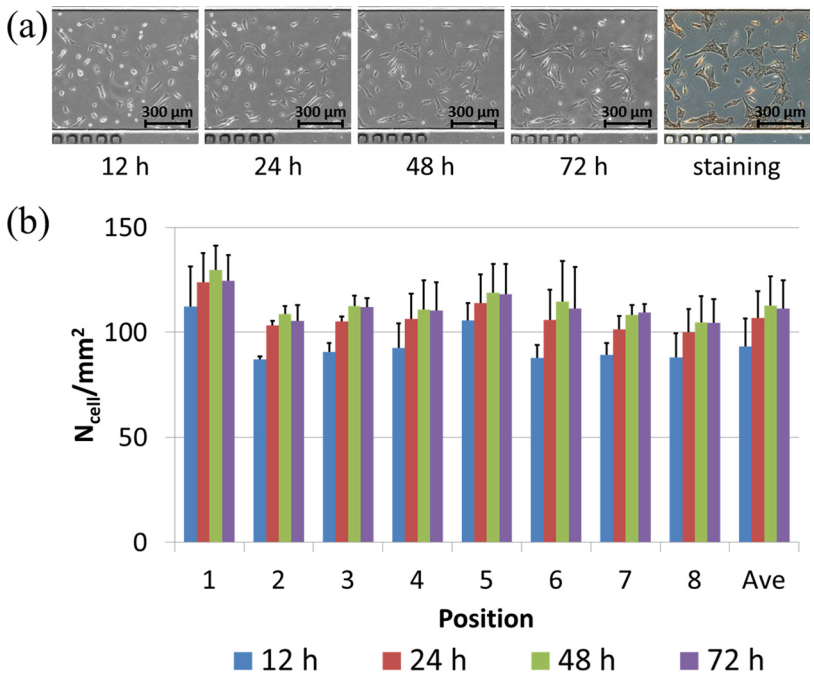

FIG. 5. (a) Microscopic pictures of VSMCs cultured on collagen coated glass substrates in a time sequence (12 h, 24 h, 48 h, and 72 h (left to right)), followed by endpoint immunostaining of alpha actin filaments. (b) Cell numbers were quantified as $93.4 \pm 13.2/mm^2$ (12 h), $106.7 \pm 12.9/mm^2$ (24 h), $112.7 \pm 13.9/mm^2$ (48 h), and $111.3 \pm 13.4/mm^2$ (72 h).

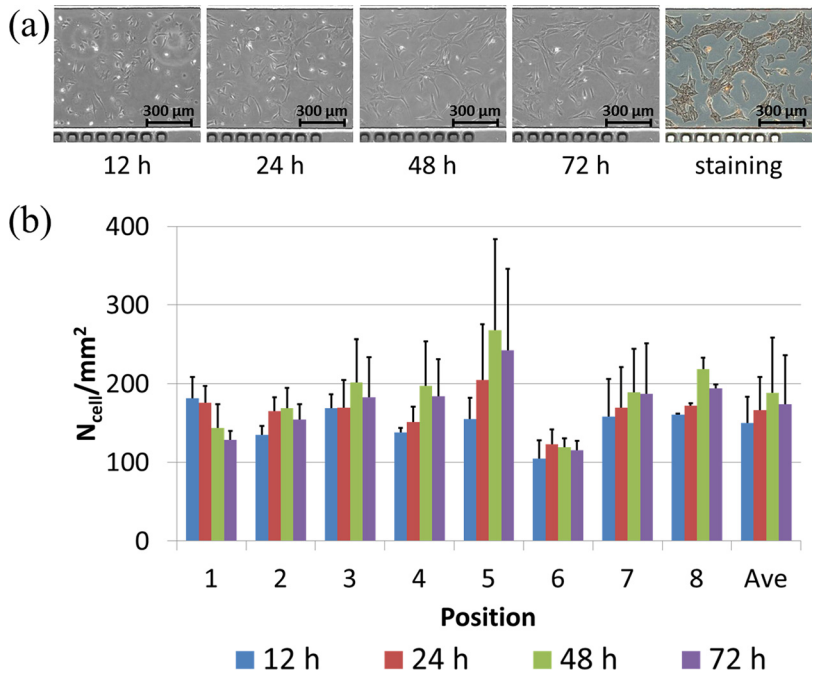

FIG. 6. (a) Microscopic pictures of VSMCs cultured on PLL coated glass substrates in a time sequence (12 h, 24 h, 48 h, and 72 h (left to right)), followed by endpoint immunostaining of alpha actin filaments. (b) Cell numbers were quantified as $150.1 \pm 33.2/mm^2$ (12 h), $166.2 \pm 42.1/mm^2$ (24 h), $188.1 \pm 70.2/mm^2$ (48 h), and $173.6 \pm 62.9/mm^2$ (72 h).

Figure 7(a) shows the microscopic images of VSMCs cultured on fibronectin coated glass substrates in a time sequence, followed by an endpoint immunostaining of alpha actin filaments. Based on the manual cell counting, the cell numbers were quantified as $111.9 \pm 13.4/mm^2$

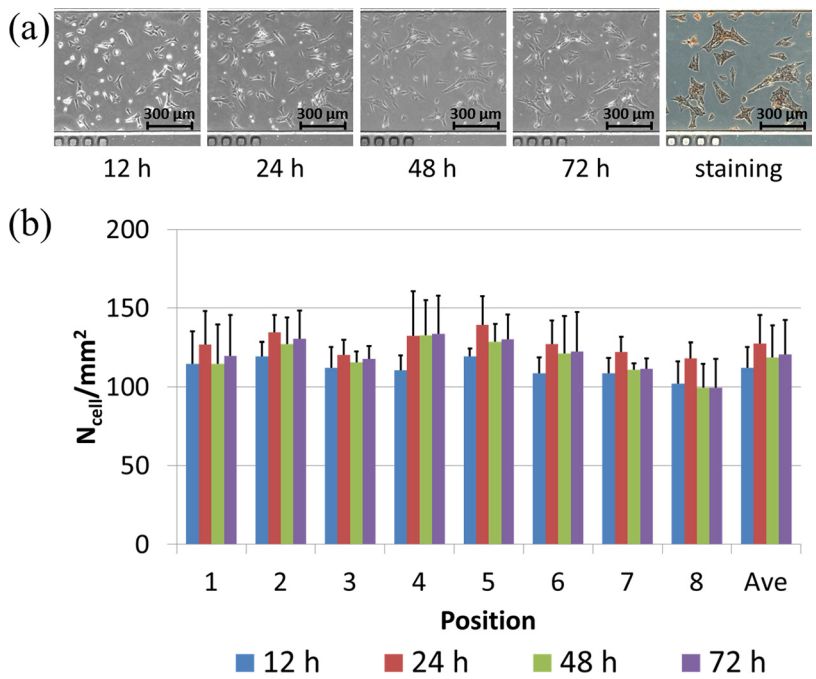

FIG. 7. (a) Microscopic pictures of VSMCs cultured on fibronectin coated glass substrates in a time sequence (12 h, 24 h, 48 h, and 72 h (left to right)), followed by endpoint immunostaining of alpha actin filaments. (b) Cell numbers were quantified as $111.9 \pm 13.4/mm^2$ (12 h), $127.5 \pm 18.0/mm^2$ (24 h), $118.8 \pm 20.0/mm^2$ (48 h) and $120.6 \pm 21.8/mm^2$ (72 h).

(12 h), $127.5 \pm 18.0/mm^2$ (24 h), $118.8 \pm 20.0/mm^2$ (48 h), and $120.6 \pm 21.8/mm^2$ (72 h) (see Figure 7(b)).

Within the first 24 h of cell seeding, noticeable VSMC proliferations were located with quantified cell numbers increased from $111.9 \pm 13.4/mm^2$ (12 h) to $127.5 \pm 18.0/mm^2$ (48 h), as an indicator of the synthetic phenotype. From 24 h to 48 h, a decrease in cellular proliferation was noticed ($127.5 \pm 18.0/mm^2$ (24 h) vs. $118.8 \pm 20.0/mm^2$ (48 h)), suggesting that VSMCs change from the synthetic phenotype to the contractile phenotype, which was further confirmed by the following 24 h with no significant cellular proliferation ($118.8 \pm 20.0/mm^2$ (48 h) vs. $120.6 \pm 21.8/mm^2$ (72 h)).

In summary, for VSMCs cultured in microfluidic channels coated with extracellular matrix (e.g., collagen, PLL, and fibronectin), cellular proliferations were initially noticed, followed by stable cell numbers without cell doubling, indicating that VSMCs changed from the synthetic phenotype to the contractile phenotype. Since cells in the middle areas of the microchannels with limited access to fresh medium (positions 4 and 5) and cells in the areas close to channel ports with easy access to fresh medium (positions 1 and 8) demonstrated similar trends (Figures 5(b), 6(b), and 7(b)), these proliferation rate variations and phenotype transitions have no relationship with nutrition transportation. Thus it was speculated that the height of microfluidic channels (100 μm) may provide geometry limitations[53] or the thickness of PDMS (2 mm) may limit oxygen transportation,[54] which was responsible for cellular proliferation and phenotype variations.

IV. CONCLUSION

This paper presented a tubing-free microfluidic platform for VSMC culture where extracellular matrix coating, VSMC seeding, culture and observation, and immunostaining were demonstrated. Based on operation optimization, even distributions of cells within microfluidic channels ($96.0 \pm 16.3/mm^2$) was realized. Compared to bare glass surface, extracellular matrix (e.g., collagen, PLL, and fibronectin) coated substrates lead to VSMC proliferations and phenotype variations in a time sequence. As a platform technology, this microfluidic device was confirmed to be capable of functioning as a new VSMC culture model for VSMC studies.

ACKNOWLEDGMENTS

The authors would like to acknowledge financial support from National Basic Research Program of China (973 Program, Grant No. 2014CB744602), Special Financial Grant from the China Postdoctoral Science Foundation (Grant No. 2013T60950), Natural Science Foundation of China (Grant Nos. 81261120561 and 61201077), National High Technology Research and Development Program of China (863 Program, Grant No. 2014AA093408) and Beijing NOVA Program.

[1]U. Hedin, J. Roy, and P. K. Tran, "Control of smooth muscle cell proliferation in vascular disease," Curr. Opin. Lipidol. **15**, 559–565 (2004).
[2]A. W. Clowes, M. M. Clowes, J. Fingerle, and M. A. Reidy, "Regulation of smooth muscle cell growth in injured artery," J. Cardiovasc. Pharmacol. **14**, S12–S15 (1989).
[3]E. Gillis, L. V. Laer, and B. L. Loeys, "Genetics of thoracic aortic aneurysm: At the crossroad of transforming growth factor-beta signaling and vascular smooth muscle cell contractility," Circ. Res. **113**, 327–340 (2013).
[4]R. W. Thompson, S. Liao, and J. A. Curci, "Vascular smooth muscle cell apoptosis in abdominal aortic aneurysms," Coron. Artery Dis. **8**, 623–631 (1997).
[5]A. Rudijanto, "The role of vascular smooth muscle cells on the pathogenesis of atherosclerosis," Acta Medica Indonesiana **39**, 86–93 (2007).
[6]E. W. Raines and R. Ross, "Smooth muscle cells and the pathogenesis of the lesions of atherosclerosis," British Heart J. **69**, S30–S37 (1993).
[7]A. I. Gotlieb, "Smooth muscle and endothelial cell function in the pathogenesis of atherosclerosis," Can. Med. Assoc. J. **126**, 903–908 (1982).
[8]S. O. Marx, H. Totary-Jain, and A. R. Marks, "Vascular smooth muscle cell proliferation in restenosis," Circ.: Cardiovasc. Interventions **4**, 104–111 (2011).
[9]V. Andres, "Control of vascular smooth muscle cell growth and its implication in atherosclerosis and restenosis (review)," Int. J. Mol. Med. **2**, 81–89 (1998).
[10]D. Proudfoot and C. Shanahan, "Human vascular smooth muscle cell culture," Methods Mol. Biol. **806**, 251–263 (2012).

[11]M. Absher, J. Woodcock-Mitchell, J. Mitchell, L. Baldor, R. Low, and D. Warshaw, "Characterization of vascular smooth muscle cell phenotype in long-term culture," In Vitro Cell. Dev. Biol.: J. Tissue Cult. Assoc. **25**, 183–192 (1989).
[12]G. M. Whitesides, "The origins and the future of microfluidics," Nature **442**, 368–373 (2006).
[13]R. C. Wootton and A. J. Demello, "Microfluidics: Exploiting elephants in the room," Nature **464**, 839–840 (2010).
[14]E. K. Sackmann, A. L. Fulton, and D. J. Beebe, "The present and future role of microfluidics in biomedical research," Nature **507**, 181–189 (2014).
[15]E. W. Young and D. J. Beebe, "Fundamentals of microfluidic cell culture in controlled microenvironments," Chem. Soc. Rev. **39**, 1036–1048 (2010).
[16]I. Meyvantsson and D. J. Beebe, "Cell culture models in microfluidic systems," Annu. Rev. Anal. Chem. **1**, 423–449 (2008).
[17]H. Ma, H. Xu, and J. Qin, "Biomimetic tumor microenvironment on a microfluidic platform," Biomicrofluidics **7**, 11501 (2013).
[18]D. Wlodkowic and J. M. Cooper, "Tumors on chips: Oncology meets microfluidics," Curr. Opin. Chem. Bio. **14**, 556–567 (2010).
[19]A. K. Soe, S. Nahavandi, and K. Khoshmanesh, "Neuroscience goes on a chip," Biosens. Bioelectron. **35**, 1–13 (2012).
[20]K. H. Wong, J. M. Chan, R. D. Kamm, and J. Tien, "Microfluidic models of vascular functions," Annu. Rev. Biomed. Eng. **14**, 205–230 (2012).
[21]A. D. van der Meer, A. A. Poot, M. H. Duits, J. Feijen, and I. Vermes, "Microfluidic technology in vascular research," J. Biomed. Biotechnol. **2009**, 823148 (2009).
[22]A. Goessl, D. F. Bowen-Pope, and A. S. Hoffman, "Control of shape and size of vascular smooth muscle cells in vitro by plasma lithography," J. Biomed. Mater. Res. **57**, 15–24 (2001).
[23]R. G. Thakar, F. Ho, N. F. Huang, D. Liepmann, and S. Li, "Regulation of vascular smooth muscle cells by micropatterning," Biochem. Biophys. Res. Commun. **307**, 883–890 (2003).
[24]A. Thapa, T. J. Webster, and K. M. Haberstroh, "Polymers with nano-dimensional surface features enhance bladder smooth muscle cell adhesion," J. Biomed. Mater. Res., Part A **67A**, 1374–1383 (2003).
[25]D. C. Miller, A. Thapa, K. M. Haberstroh, and T. J. Webster, "Endothelial and vascular smooth muscle cell function on poly(lactic-co-glycolic acid) with nano-structured surface features," Biomaterials **25**, 53–61 (2004).
[26]N. Zaari, P. Rajagopalan, S. K. Kim, A. J. Engler, and J. Y. Wong, "Photopolymerization in microfluidic gradient generators: Microscale control of substrate compliance to manipulate cell response," Adv. Mater. **16**, 2133–2137 (2004).
[27]J. D. Glawe, J. B. Hill, D. K. Mills, and M. J. McShane, "Influence of channel width on alignment of smooth muscle cells by high-aspect-ratio microfabricated elastomeric cell culture scaffolds," J. Biomed. Mater. Res., Part A **75A**, 106–114 (2005).
[28]S. Sarkar, M. Dadhania, P. Rourke, T. A. Desai, and J. Y. Wong, "Vascular tissue engineering: microtextured scaffold templates to control organization of vascular smooth muscle cells and extracellular matrix," Acta Biomater. **1**, 93–100 (2005).
[29]E. K. F. Yim, R. M. Reano, S. W. Pang, A. F. Yee, C. S. Chen, and K. W. Leong, "Nanopattern-induced changes in morphology and motility of smooth muscle cells," Biomaterials **26**, 5405–5413 (2005).
[30]J. Y. Shen, M. B. Chan-Park, Z. Q. Feng, V. Chan, and Z. W. Feng, "UV-embossed microchannel in biocompatible polymeric film: Application to control of cell shape and orientation of muscle cells," J. Biomed. Mater. Res., Part B **77B**, 423–430 (2006).
[31]J. Y. Shen, M. B. Chan-Park, B. He, A. P. Zhu, X. Zhu, R. W. Beuerman *et al.*, "Three-dimensional microchannels in biodegradable polymeric films for control orientation and phenotype of vascular smooth muscle cells," Tissue Eng. **12**, 2229–2240 (2006).
[32]J. Feng, M. B. Chan-Park, J. Shen, and V. Chan, "Quick layer-by-layer assembly of aligned multilayers of vascular smooth muscle cells in deep microchannels," Tissue Eng. **13**, 1003–1012 (2007).
[33]B. D. Plouffe, D. N. Njoka, J. Harris, J. Liao, N. K. Horick, M. Radisic *et al.*, "Peptide-mediated selective adhesion of smooth muscle and endothelial cells in microfluidic shear flow," Langmuir **23**, 5050–5055 (2007).
[34]S. Chung, R. Sudo, P. J. Mack, C.-R. Wan, V. Vickerman, and R. D. Kamm, "Cell migration into scaffolds under co-culture conditions in a microfluidic platform," Lab Chip **9**, 269–275 (2009).
[35]B. C. Isenberg, P. A. Dimilla, M. Walker, S. Kim, and J. Y. Wong, "Vascular smooth muscle cell durotaxis depends on substrate stiffness gradient strength," Biophys. J. **97**, 1313–1322 (2009).
[36]R. G. Thakar, Q. Cheng, S. Patel, J. Chu, M. Nasir, D. Liepmann *et al.*, "Cell-shape regulation of smooth muscle cell proliferation," Biophys. J. **96**, 3423–3432 (2009).
[37]Y. Cao, Y. F. Poon, J. Feng, S. Rayatpisheh, V. Chan, and M. B. Chan-Park, "Regulating orientation and phenotype of primary vascular smooth muscle cells by biodegradable films patterned with arrays of microchannels and discontinuous microwalls," Biomaterials **31**, 6228–6238 (2010).
[38]S. Rayatpisheh, Y. F. Poon, Y. Cao, J. Feng, V. Chan, and M. B. Chan-Park, "Aligned 3D human aortic smooth muscle tissue via layer by layer technique inside microchannels with novel combination of collagen and oxidized alginate hydrogel," J. Biomed. Mater. Res., Part A **98A**, 235–244 (2011).
[39]C. Williams, X. Q. Brown, E. Bartolak-Suki, H. Ma, A. Chilkoti, and J. Y. Wong, "The use of micropatterning to control smooth muscle myosin heavy chain expression and limit the response to transforming growth factor β1 in vascular smooth muscle cells," Biomaterials **32**, 410–418 (2011).
[40]R. Rodriguez-Rodriguez, X. Munoz-Berbel, S. Demming, S. Buttgenbach, M. D. Herrera, and A. Llobera, "Cell-based microfluidic device for screening anti-proliferative activity of drugs in vascular smooth muscle cells," Biomed. Microdevices **14**, 1129–1140 (2012).
[41]J. Li, K. Zhang, P. Yang, Y. Liao, L. Wu, J. Chen *et al.*, "Research of smooth muscle cells response to fluid flow shear stress by hyaluronic acid micro-pattern on a titanium surface," Exp. Cell Res. **319**, 2663–2672 (2013).
[42]J. S. Choi, Y. Piao, and T. S. Seo, "Circumferential alignment of vascular smooth muscle cells in a circular microfluidic channel," Biomaterials **35**, 63–70 (2014).
[43]Y. Zhang, S. S. Ng, Y. Wang, H. Feng, W. N. Chen, M. B. Chan-Park *et al.*, "Collective cell traction force analysis on aligned smooth muscle cell sheet between three-dimensional microwalls," Interface Focus **4**, 20130056 (2014).

[44]J. P. Puccinelli, X. Su, and D. J. Beebe, "Automated high-throughput microchannel assays for cell biology: Operational optimization and characterization," J. Assoc. Lab. Autom. **15**, 25–32 (2010).
[45]I. Meyvantsson, J. W. Warrick, S. Hayes, A. Skoien, and D. J. Beebe, "Automated cell culture in high density tubeless microfluidic device arrays," Lab Chip **8**, 717–724 (2008).
[46]G. Walker and D. J. Beebe, "A passive pumping method for microfluidic devices," Lab Chip **2**, 131–134 (2002).
[47]S. Takayama, J. C. McDonald, E. Ostuni, M. N. Liang, P. J. A. Kenis, R. F. Ismagilov *et al*., "Patterning cells and their environments using multiple laminar fluid flows in capillary networks," Proc. Natl. Acad. Sci. U. S. A. **96**, 5545–5548 (1999).
[48]S. Takayama, E. Ostuni, P. LeDuc, K. Naruse, D. E. Ingber, and G. M. Whitesides, "Subcellular positioning of small molecules," Nature **411**, 1016 (2001).
[49]S. Takayama, E. Ostuni, P. LeDuc, K. Naruse, D. E. Ingber, and G. M. Whitesides, "Selective chemical treatment of cellular microdomains using multiple laminar streams," Chemistry and Biology **10**, 123–130 (2003).
[50]P. L. Weissberg, N. R. Cary, and C. M. Shanahan, "Gene expression and vascular smooth muscle cell phenotype," Blood Pressure, Suppl. **2**, 68–73 (1995).
[51]I. P. Hayward, K. R. Bridle, G. R. Campbell, P. A. Underwood, and J. H. Campbell, "Effect of extracellular matrix proteins on vascular smooth muscle cell phenotype," Cell Biol. Int. **19**, 839–846 (1995).
[52]J. P. Stegemann, H. Hong, and R. M. Nerem, "Mechanical, biochemical, and extracellular matrix effects on vascular smooth muscle cell phenotype," J. Appl. Physiol. **98**, 2321–2327 (2005).
[53]H. Yu, I. Meyvantsson, I. A. Shkel, and D. J. Beebe, "Diffusion dependent cell behavior in microenvironments," Lab Chip **5**, 1089–1095 (2005).
[54]E. Leclerc, Y. Sakai, and T. Fujii, "Cell culture in 3-Dimensional microfluidic structure of PDMS (polydimethylsiloxane)," Biomed. Microdevices **5**, 109–114 (2003).